The Globular Cluster System of the Auriga Simulations

Timo L. R. Halbesma[1]⋆, Robert J. J. Grand[1], Volker Springel[1], Facundo A. Gómez[2,3], Federico Marinacci[4,5], Rüdiger Pakmor[1], Wilma Trick[1], Philipp Busch[1], Simon D. M. White[1]

[1] *Max-Planck-Institut für Astrophysik, Karl-Schwarzschild-Str. 1, 85741 Garching, Germany*
[2] *Instituto de Investigación Multidisciplinar en Ciencia yTecnología, Universidad de La Serena, Raúl Bitrán 1305, La Serena, Chile*
[3] *Departamento de Física y Astronomía, Universidad de La Serena, Av. Juan Cisternas 1200 N, La Serena, Chile*
[4] *Department of Physics, Kavli Institute for Astrophysics and Space Research, MIT, Cambridge, MA 02139, USA*
[5] *Harvard-Smithsonian Center for Astrophysics, 60 Garden Street, Cambridge, MA 02138, USA*

ABSTRACT

Rob Grand: 'for many Auriga papers Carlos Frenk and Adrian Jenkins are offered co-authorship. Perhaps you could ask Simon about this.'

We investigate whether the galaxy formation model used for the Auriga simulations can produce a realistic globular cluster population at redshift zero. We compare properties of the simulated star particles in the Auriga haloes with catalogues of observations of the Milky Way globular cluster population available in the literature. We find that the Auriga simulations do produce sufficient mass at radii and metallicities that are typical for the MW GCS, although we observe a varying mass-excess for the different R_{GC}-[Fe/H] bins. This implies different values for the combined product of the bound cluster formation efficiency and the globular cluster disruption rate. We investigate whether these differences could result from formation insitu vs. accreted star particles. We find ... TODO. Furthermore we test whether any of the Auriga galaxies has a metallicity and radial distribution that is consistent with the MW (M31) GCS. For all of the Auriga haloes we reject the null hypothesis that the simulated and observed metallicities are drawn from the same distribution at $\geq$ 98.32 % confidence level, for the GCS of the Milky Way as well as that of the Andromeda galaxy. The same holds true for the distribution of galactocentric radius.

Key words: methods: numerical – galaxies: formation – galaxies: star clusters: general.

1 INTRODUCTION

Globular clusters (GC)s are omnipresent, bright, old, and amongst the simplest stellar configurations in the Universe. The globular cluster systems (GCS) of the Milky Way (MW) and the Andromeda galaxy (M31) have been studied extensively over the last decades. More recent analyses of the Gaia data shed new light on the chemical- and structural properties, and on the phase-space distribution of the MW GC system. Moreover, the visbility and ubiquity of GCs makes it possible to obtain integrated properties of GCs within the Local Group with reasonable certainty, and even of those that are located further away within the Virgo Supercluster.

The natal gas regions in which globular clusters form inherit key characteristics from their parent (proto-)galaxies. GC populations, in turn, will therefore retain a record of these properties and offer unique insight into the detailed chemical and dynamical evolution history of their host galaxies. In theory, this information should be readily available and easily observable in the low redshift Universe, given that GCs survive nearly a Hubble time of evolution within the violent galactic environments they live in. However, these long and complex evolution histories themselves imposes their imprints onto the GCs observables. Thus, a prerequisite to infer galactic histories from studies of GC systems is to understand the subtleties of the GC formation and evolution itself.

The literature offers several formation scenerarios that are consistent with the data. One important constraint comes from bimodality in the colour distribution, which is indicative of a bimodality in the underlying metallicity distribution of GC systems. For example, GCs in the MW are typically split up in a metal-rich (red) and metal-poor (blue) subpopulation divided at [Fe/H] = −1 (e.g. Harris 2001). These two subpopulations could be associated to the galactic disk, respectively to the stellar halo (e.g. Zinn 1985). The

---

⋆ E-mail: Halbesma@MPA-Garching.MPG.DE

latter is supported by observed similarities between the spatial distribution and chemical signature of the 'blue' GCs and the Galactic stellar halo (Helmi 2008). Moreover, relative age-estimates indicate that the metal-poor subpopulation may be 1.5 Gyr younger than the metal-rich counterpart (De Angeli et al. 2005), providing futher support that the GC population indeed consists of two distinct classes.

People postulate that the frequent mergers that occur during hierarchical build-up of galaxies naturally produce (sub)populations of GCs from enriched gas on tight orbits, if the mass ratios and gas fractions of the mergers are sufficiently high.

Boylan-Kolchin: the blue population could form in high density regions along the cosmic filament before or during the collapse of the proto-galaxy itself. This formation scenario would explain the presence of the oldest GCs with primordial metallicities in the (outer) haloes of galaxies as the GCs are accreted over time. Moreover, the tidal fields experienced by GCs at (outer) halo orbits is significantly lower than by GCs in the inner galaxy, thus such GCs are expected to be long-lived.

In a recent study, Chiou et al. speculate that GCs may form in supersonically induced gasseous objects at high redshifts. These objects are free of dark matter and populate a mass range consistent with the typical mass scale of GCs. Interestingly, the authors find present-day absolute visual magnitude and characteristic scales consistent with GCs in the Local group, based on a rudimentary star formation model.

An alternative paradigm is that GC formation does not rely on special conditions at high redshifts. Rather, the same physics that governs the formation of young massive clusters (YMCs) in the Local Group can be applied to the high redshift Universe. The observed differences between YMCs and GCs, in this scenario, arise naturally as the result intrinsic GC evolution within galactic tidal fields over a Hubble time. This interesting hypothesis is tested numerically by the E-MOSAICS people.

Brodie & Strader (2006) for a review of extragalactic GCs and galaxy formation.

- Special conditions in early Universe?
- Formation in collapsing proto-galaxies (in-situ-ish?)
- Formation as a result of (wet) mergers?
- Formation in satellites that are later accreted?
- No special conditions at high z, but connection between low-z YMC- and high-z GC-formation where differences could result from Hubble time of evolution?
- This means that in order to test formation models against observations, one not only needs needs to model GC formation, but also include the full evolution over their lifetime in a cosmological tidal field.

Paragraph: ingredients for numerical studies

- High resolution in the ISM
- Full cosmological evolution

Paragraph: narrow down to this work

- The star formation model implemented in the Auriga simulations is capable of producing a suite/population of realistic Milky Way-like galaxies at redshift zero.
- Therefore the question naturally arises whether or not the Auriga simulations are also capable of faithfully producing a globular cluster population as observed in the Milky Way (or Andromeda).
- Globular cluster formation in cosmological zoom simulations

is very interesting for two reasons. First of all, extragalactic observations typically show the integrated properties of globular clusters rather than that of the individual stars within the clusters. Moreover, the typical mass scale of globular clusters is comparable to the numerical (mass) resolution of cosmological zoom simulations. The detailed small scale physics that is at play for real world globular clusters appears in observations as the combined effect of the 10^{3-6} M$_\odot$, compared to a mass resolution of 10^{3-5} M$_\odot$ for the Auriga simulations. Globular clusters can therefore serve as an ultimate test to the star formation model that is implemented in the numerical simulations. Secondly, cosmological zoom simulations provide an accurate recording of the full and detailed merger history of the simulated galaxy. This is important because theoretical paradigms for globular cluster formation in the literature know two distinct classes of GCs that are separated by their exact formation sites: an in-situ versus an accreted population. Cosmological zoom simulations uniquely allow for an investigation into globular cluster formation with particular focus on the in-situ and accreted populations.

Paragraph: Paper outline

We summarise the relevant characteristics of the Auriga simulations in section 2, followed by a summary of the observations of the Milky Way (MW) globular cluster system (GCS) in section 3 that we use to compare our simulations to in section 4. We discuss our findings in section 5 to come to our conclusions in section 6.

2 THE AURIGA SIMULATIONS

We use the Auriga simulations (Grand et al. 2017, hereafter G17), a suite of high-resolution cosmological zoom simulations of Milky Way-mass selected initial conditions. The simulations are performed with the state-of-the art code AREPO (Springel 2010; Pakmor et al. 2016), that solves the magnetohydrodynamical equations on a moving mesh, and an elaborate galaxy formation model that produces realistic spiral galaxies at redshift $z = 0$.

The interstellar medium is modelled using a sub-grid approach which implements the physical processes most relevant to galaxy formation and evolution. This model was tailored to the AREPO code and calibrated to reproduce key observables of galaxies, such as the history of the cosmic star formation rate density, the stellar mass to halo mass relation, and galaxy luminosity functions.

The sub-grid includes primordial and metal-line cooling with self-shielding corrections. Reionization is completed at redshift six by a time-varying spatially uniform UV background (Faucher-Giguère et al. 2009; Vogelsberger et al. 2013) The interstellar medium is described by an equation of state for a two-phase medium in pressure equilibrium (Springel & Hernquist 2003) with stochastic star formation in thermally unstable gas with a density threshold of $n = 0.13 \text{cm}^{-3}$, and consecutive stellar evolution is accounted for. Stars provide feedback by stellar winds (Marinacci et al. 2014; Grand et al. 2017), and further enrich the ISM with metals from SNIa, SNII, and AGB stars (Vogelsberger et al. 2013). The formation of black holes is modelled which results in feedback from active galactic nuclei (Springel et al. 2005; Marinacci et al. 2014; Grand et al. 2017). Finally, the simulations follow the evolution of a magnetic field of 10^{-14} (comoving) G seeded at $z = 127$ (Pakmor & Springel 2013; Pakmor et al. 2014). See G17 for further details of the numerical setup as well as the galaxy formation model.

The Auriga suite has a fiducial resolution level L4, accompanied by the lower (higher) level L5 (L3) that is available for selected

initial condition runs. The baryonic mass resolution in order of increasing level is $m_b = [4 \times 10^5, 5 \times 10^4, 6 \times 10^3]\,M_\odot$ with gravitational softening of collissionless particles $\epsilon = [738, 369, 184]$ pc.

3 OBSERVATIONAL DATA

We describe the observations of the MW GCS in Sec. 3.1, and of the Andromeda (M31) GCS in Sec. 3.2

3.1 Milky Way

Harris (1996, 2010 edition; hereafter H96e10) provides a catalogue[1] of the Milky Way globular cluster system that contains properties of 157 GCs. The authors initially estimated the size of the MW GCS to be 180 ± 10, thus, their catalogue to be ~85% complete. However, an additional 59 GCs have since been discovered by various authors. The total confirmed number of GCs in the MW adds up to 216 with new estimates now anticipating an additional thirty GCs yet to be discovered (e.g. Ryu & Lee 2018, and references therein). We still use data from the Harris catalogue, but caution that it may (only) be 53-72% complete. Specifically, the relevant data fields that we use from H96e10 are the metallicity [Fe/H], the Galactic distance components X, Y, and Z (in kpc)[2], and absolute magnitude in the V-band M_V. We use the latter to calculate mass-estimates by assuming $M_{V,\odot} = 4.83$ and a mass to light ratio $M/L_V = 1.7\,M/L_\odot$, the mean for MW clusters (McLaughlin & van der Marel 2005).

We supplement the catalogue with age-estimates from isochrone fits to stars near the main-sequence turnoff in 55 GCs (VandenBerg et al. 2013, hereafter V13). The mean value of the age-estimates in this data set is 11.9 ± 0.1 Gyr and the dispersion is 0.8 Gyr. Furthermore, only one of the 55 GC age-estimates is below 10 Gyr.

3.2 Andromeda

The fifth revision of the revised bologna catalogue (RBC 5, last updated August, 2012) is the latest edition of three decades of systematically collecting integrated properties of the globular cluster system of the Andromeda galaxy (Galleti et al. 2004, and references therein). One contribution to RBC 5 is the work by Caldwell et al. (2011, hereafter C11), subsequently updated by Caldwell & Romanowsky (2016, hereafter CR16).

C11 and CR16 present a uniform set of spectroscopic observations calibrated on the Milky Way GCS of the inner $1.6°$ (~ 21) kpc that is believed to be 94% complete. GCs in the outer stellar halo, up to $R_{proj} \sim 150$ kpc, are observed in the Pan-Andromeda Archaeological Survey (PAndAS, Huxor et al. 2014, hereafter H14), but see also Veljanoski et al. (2014) and Mackey et al. (2019). H14 presents the discovery of 59 new GCs and publishes updates to RBC 5. The work of H14 is incorporated in the latest public release[3] of the C11 dataset, further revised by CR16. It seems that CR16 is the most recent aggregated dataset of M31's GCS that contains properties of interest for our study as it contains GCs in the inner region and in
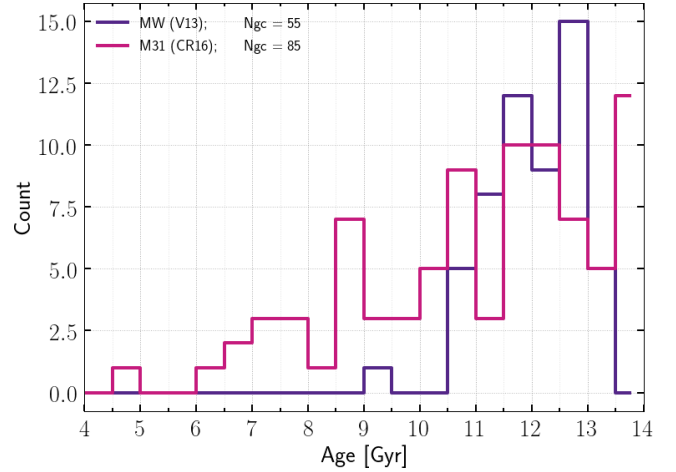

Figure 1. Age distribution of 55 GCs in the MW (data from VandenBerg et al. 2013) and 88 GCs in M31 (data from Caldwell & Romanowsky 2016).

the outer halo. The relevant fields in the CR16 dataset that we use are the age, metallicity, and the mass-estimate[4].

The M31 GCS has a mean age of 11.0 ± 0.2 Gyr with a dispersion of 2.2 Gyr, and 24 GCs have age-estimates below 10 Gyr with a minimum age of 4.8 Gyr. We show a histogram of the age-estimates of the 55 MW GCs in V13 and 88 GCs in M31 for which age-estimates are available in CR16, see Figure 1.

3.3 Total GC mass in metallicity-radial space

We show the two-dimensional mass-weighted metallicity-radial distribution of the MW (M31) GCS in the top (bottom) panel of Figure 2. Both quantities are readily available in H96e10 (assuming $R_\odot = 8.0$ kpc), but the galactocentric radius of GCs in M31 is not available in CR16. Therefore we follow Wang et al. (2019, Sec. 4.1) to calculate the projected radius R_{proj} from the observed positions, adopting M31's central position from the NASA Extragalactic Database[5] $(\alpha_0, \delta_0) = (0^h 42^m 44.35^s, +41° 16' 08.63")$ and distance $D_{M31} = 778$ kpc (McConnachie et al. 2005; Conn et al. 2012). We calculate R_{GC} as 'average deprojected distance' $R_{GC} = R_{proj} \times (4/\pi)$. The observations indicate that no GCs with high metallicities are to be expected at large radii (the three bins in the upper right corner, both for MW and M31), and relatively few GCs at large radii in general ($R_{GC} > 30$ kpc; right column: 11 GCs or 7.3% in the MW and 17 or 4.6% in M31). We compare these observations to the Auriga simulations later on in Sec. 4.3.

4 RESULTS

We define GC candidates in the Auriga simulations as all star particles older than 10 Gyr based on the age distribution of the MW GCS (Figure 1), and following the analysis of Renaud et al. (2017).

Trough out our analysis we compare the distributions of three subsets of star particles: *old stars* (age > 10 Gyr, or GC candidates), *old insitu* stars (defined as those bound to the most-massive halo/subhalo in the first snapshot that the particle was recorded),

---

[1] See https://www.physics.mcmaster.ca/Fac_Harris/mwgc.dat
[2] In a Sun-centered coordinate system: X points toward Galactic center, Y in direction of Galactic rotation, and Z toward the North Galactic Pole. We calculate the galactocentric radius $R_{GC} = \sqrt{(X - R_\odot)^2 + Y^2 + Z^2}$, assuming the solar radius $R_\odot = 8$ kpc.
[3] Last revised 23 Sep 2015, see https://www.cfa.harvard.edu/oir/eg/m31clusters/M31_Hectospec.html

[4] The authors assumed $M/L_V = 2$ independent of [Fe/H]
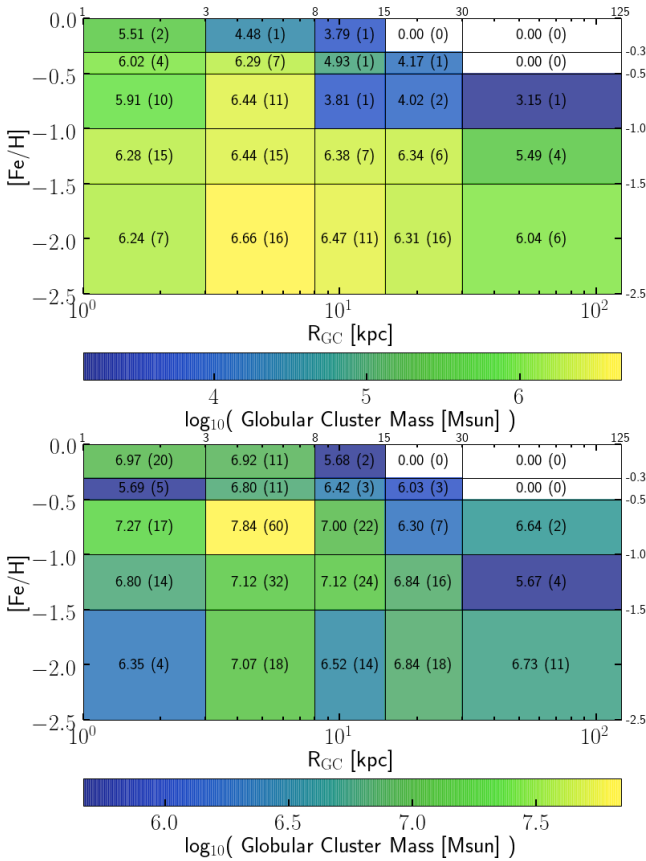[5] https://ned.ipac.caltech.edu/

Figure 2. *Top*: Mass-weighted R_{GC}-[Fe/H] distribution of 151 GCs in the MW (data from Harris 1996, 2010 ed.), which is 98.19 % of the total MW GCS mass in the Harris catalog. *Bottom*: Same for M31, showing 366 GCs and 88.38 % of the total mass in CR16 (data from Caldwell & Romanowsky 2016). Note that the range of the colourmap differs in both figures.

and *old accreted* star particles (those that have formed ex-situ and are bound to the most-massive halo/subhalo at $z = 0$). For comparison we also include the results for *all stars* (when no additional selection criterion is applied to the star particles). We consider the metallicity distribution in Sec. 4.1, the distribution of galactocentric radii in Sec. 4.2, and the combination of both in Sec. 4.3.

4.1 Metallicity distribution

We investigate whether the star formation model implemented in Auriga produces metallicity distributions consistent with the MW (M31) GC system, and whether the subgrid generates sufficient total mass at metallicities typical for the MW (M31) GCS.

Figure 3 shows the normalized metallicity distribution of Au4-10[6] and Au4-21, showing the GC candidates in green. The accreted GC candidates are shown in red, and the insitu subpopulation in blue. The top panels show the MW (M31) GC system in purple (magenta). We overplot a double Gaussian for the MW GCS (the purple dashed lines), adopting literature values of the

---

[6] The nomenclature is 'Au' for Auriga, followed by the resolution level (4) and halo number (10 - indicating which set of initial conditions was used the run).

mean μ and standard deviation σ of the metal-rich and metal-poor populations (Harris 2001, p. 38).

We find that the age cut lowers the mean metallicity from ~0.0 to ~−0.6. Furthermore, the old accreted stars generally have lower metallicities than the old insitu stars. The difference between the mean metallicity of the old insitu and old accreted stars for the majority of the simulations is ~0.3 (e.g. Au4-21), and ~0.5 dex for Au4-10, Au4-16, Au4-17, Au4-18 and Au4-22. This trend is only reversed for Au4-1 and Au4-4, for which the old insitu population has a lower mean metallicity instead. For Au4-1 we find $\mu = -1.51$ (-0.74) for the old insitu (accreted), but the former consists of only 1019 particles (1.3% of all GC candidates, and with a total mass of 5e7 $M_\odot$) thus we believe our classification of insitu is flawed for this halo due to misclassification of the primary halo in the merger tree by subfind. For Au4-4, 10.8 % of the GC candidates is classified as insitu (compared to insitu fractions of 40 − 80% for other haloes). Overall we find that the simulations produce (sub)populations of GC candidates that are more metal-rich than the MW and M31 GC systems. Moreover, none of the simulations has a population of GC candidates with a bimodal metallicity distribution (the green curves).

We show the mean metallicity and standard deviation of all thirty Auriga L4 haloes in Figure 4. The green crosses are to be compared to the purple (magenta) cross, which shows the mean value of all MW (M31) GCs. We test the null hypothesis that MW (M31) and the GC candidates (all, insitu, and accreted) are drawn from the same underlying distribution by calculating the KS test statistic (i.e. six KS tests per simulation). We reject H_0 at the 100.00 % confidence level for virtually all subsets of all simulations, both for MW and M31, except when comparing the old accreted stars of Au4-10 to the MW GCS. In this case we still reject H_0 with, but with ≤ 98.68 % confidence. When comparing to the M31 GCS, the 'best' matches are the old accreted subpopulations of Au4-13, Au4-15, and Au4-17 (H_0 rejected with ≤ 99.82 % confidence, 99.95 %, and 98.32 %). Here we find that the cumulative distributions are more or less similar up to [Fe/H] ~−0.5, above which the simulations yield higher number counts which drives the KS test statistic over the critical values. This affirms our finding that the simulations produce GC candidates that are more metal-rich than the MW (M31) GCS. The main reason reasons that H_0 is rejected with such high confidence are under-production of old stars with [Fe/H] ≤ -1.5, and over-production of stars with [Fe/H] ≥ -0.5.

In addition, we show the metal-rich (metal-poor) population of the MW GCS using a solid (open) dot. The mean metallicities of the old insitu populations appear roughly consistent with that of the metal-rich population of the MW, but the simulations show larger dispersions. We are uncertain whether definitive consensus is reached concerning uni- or bimodality in the [Fe/H] distribution of M31, but CR16 argues that the data, after removal of younger objects due to improved age classification, leans towards unimodality. Therefore we do not show two data points for the M31 GCS.

We now turn to the total mass in GC candidates produced by the Auriga simulations. We show the median (coloured lines) for all thirty Auriga L4 haloes with the 1σ interval around it (shaded regions, which shows the scatter between runs that have different initial conditions, thus, have unique merger histories). We chose to aggregate the data to indicate a general trend that we find when the GC candidates are split up according to birth location, rather than selecting typical examples of individual galaxies. Figure 5 shows the mass-weighted metallicity distribution of all Auriga L4 galaxies. Once again we notice that the peak metallicity shifts down from 0 to −0.5 for old stars (green solid) compared to all stars (green
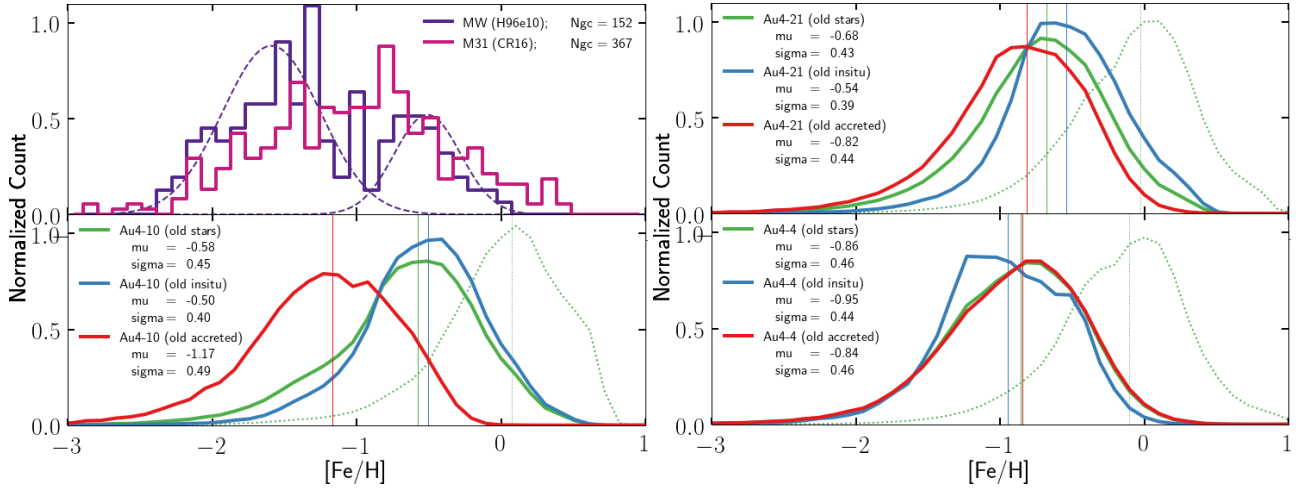
Figure 3. *Left:* Metallicity distribution of Au4-10 (bottom panel). We show the GG candicates in green. We split the GC candidates into two subpopulations, those that have formed insitu (blue), and those that have been accreted (red). The dotted green line shows all star particles. The solid purple (magenta) line in the top panel shows the GC system of the MW (M31). *Right:* Au4-4 (bottom), and Au4-21 (top).
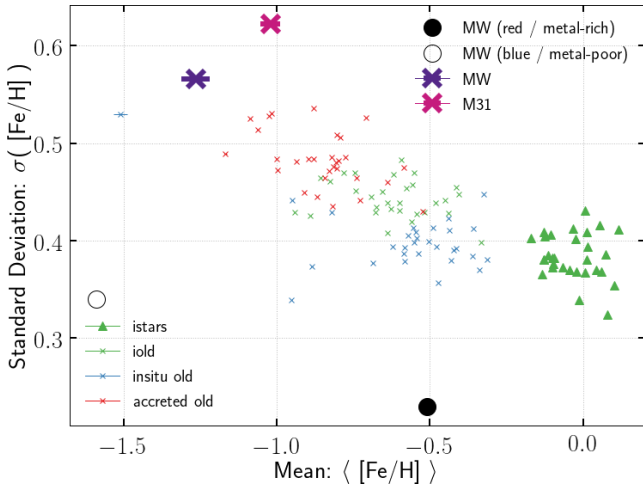

Figure 4. First vs second central moment of the Auriga L4 metallicity distributions. Each cross (for a given colour) represents one simulation. The green (blue) [red] crosses show the values calculated using the old (old insitu) [old accreted] star particles. Green triangles indicate that all stars were used. The purple (magenta) cross denotes our calculation using all MW (M31) observations (which would be appropriate for a unimodal distribution). The black solid (open) dots indicate the literature values of a bimodal Gaussian fit to the data (values from Ashman & Zepf 1998, p. 38), showing the metal-rich (metal-poor) component of the MW.

dotted), and we learn that the mass at the peak lowers by roughly one dex. The mass budget of the old stars is dominated by the old insitu population (blue solid) below $[Fe/H] = -1$, and by the old accreted stars (red solid) above this value. We show the MW (M31) GCS in purple (magenta) and we show the ratio of the simulated to the observed profiles in the middle (bottom) panel. This mass excess can be thought of the 'mass budget' that the Auriga GC candidates can 'afford to lose' due to a combination of smaller than unity bound cluster formation efficiencies combined with a Hubble time of dynamical evolution, while still producing a GC system with sufficient mass to be consistent with the MW (M31) GCS. The cluster formation efficiency would have to linearly decrease
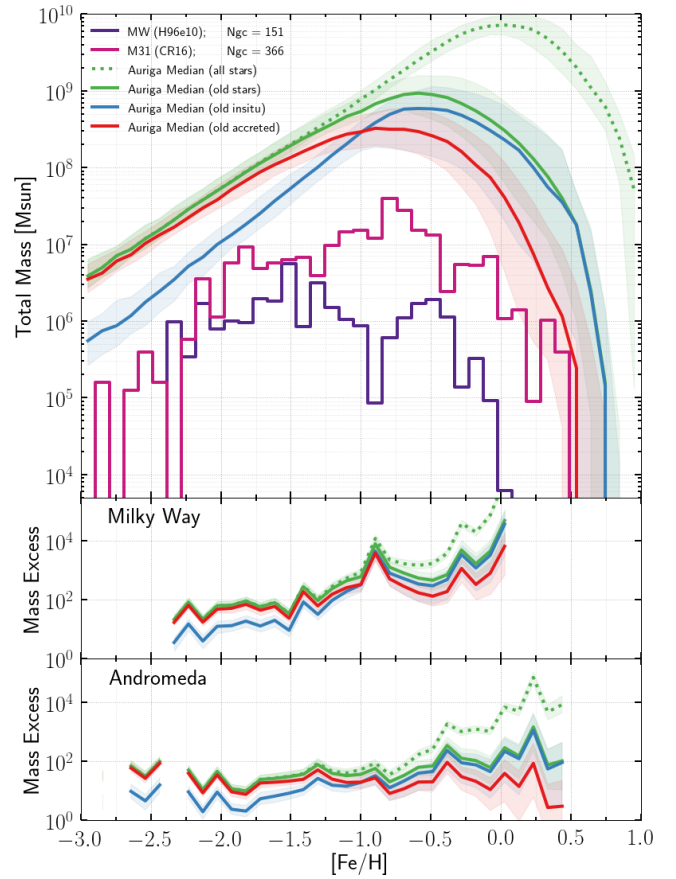

Figure 5. Mass-weighted metallicity distribution of star particles in the Auriga simulations. We show the median value of all Auriga haloes for all stars (green dotted) and globular cluster candidates (i.e. stars with age > 10 Gyr; green solid). The latter sub set is further split up between stars that formed in-situ (blue solid), and those that were accreted (red solid). Shaded regions indicate the 1σ interval. The MW (M31) GCS is shown in purple (magenta). The middle (bottom) panel shows the ratio of the simulated mass to the mass in the MW (M31) GCS.
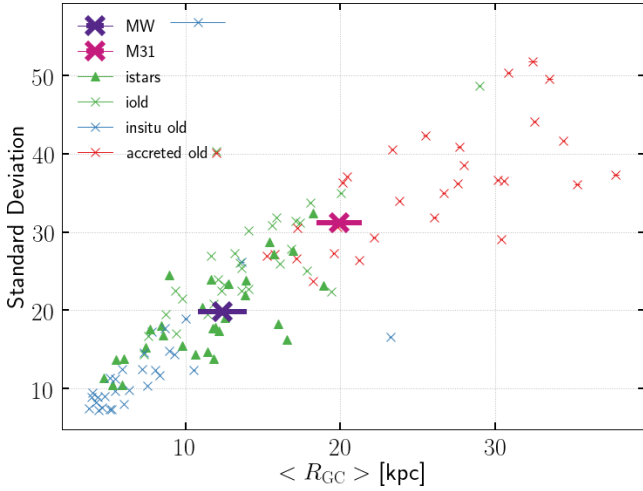
Figure 6. Mean and standard deviation of the radial distribution of star particles in each of the thirty Auriga L4 haloes compared to the MW (M31) GCS shown in purple (magenta).

with decreasing metallicity for Auriga GC candidates to produce a population of GC candidates that is consistent with the MW. For the GC candidates in M31 we find a constant mass excess up to ~-0.9, above which the simulations produce a higher mass excess with increasing metallicity. If dynamical evolution is not expected to more efficiently disrupt GCs of higher metallicity, then we would find that the efficiency to form bound star clusters would have to decrease with increasing metallicity.

4.2 Radial distribution

Figure 6 shows the mean and standard deviation of the radial distribution of star particles in all Auriga L4 simulations. We notice that the old insitu populations are much more centrally distributed, whereas the old accreted component has a larger radial extent. Moreover, the dispersion increases with increasing mean value of the radial distribution as may be expected for a quantity that cannot have negative values.

Figure 7 shows the mass-weighted radial distribution of the Auriga L4 haloes. We notice a subtle peak around 10 kpc for all star particles that is not present for the GC candidates, indicating that the stellar disc is no longer present when applying the latter selection criterion. Furthermore, we find that the dominant contribution to the total mass in GC candidates changes from those formed insitu to the accreted population around 10 kpc. Again we show the mass excess of the simulations compared to the Milky Way and Andromeda GCS. We find a decreasing mass excess with increasing radius in the range 0.2 to ~5 kpc, followed by an increase attributed to the accreted subpopulation. We further investigate a breakdown of the total mass in Auriga GC candidates into bins of both metallicity and radius in the following section.

4.3 Total mass in metallicity-radial space

We investigate whether the Auriga simulations still produce sufficient mass when the GC candidates are two-dimensionally binned in [Fe/H] and R_{GC}. First we sum the total simulated mass in each bin (for an individual Auriga simulation), then we calculate the median over all thirty Auriga L4 haloes (in each bin, see Figure 8 which
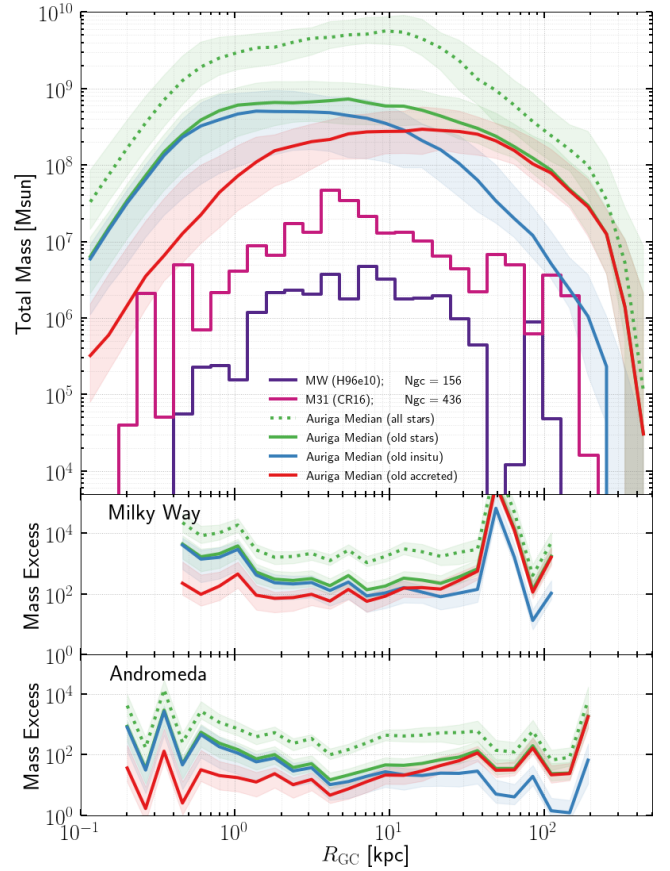

Figure 7. Mass-weighted radial distribution of star particles in the Auriga simulations. We show the median value of all Auriga haloes for all stars (green dotted) and globular cluster candidates (i.e. stars with age > 10 Gyr; green solid). The latter sub set is further split up between stars that formed in-situ (blue solid), and those that were accreted (red solid). Shaded regions indicate the 1σ interval. The MW (M31) GCS is shown in purple (magenta). The middle (bottom) panel shows the ratio of the simulated mass to the mass in the MW (M31) GCS.

can be compared to Figure 2). Finally, we divide these value by the total mass in the MW (M31) GCS to obtain the median mass excess produced by the star formation model implemented in the Auriga simulations. See the top (bottom) panel of Figure 8 for mass excess with respect to the MW (M31) GCS.

5 DISCUSSION

5.1 Metallicity distribution

Ashman & Zepf (1998, p. 234) and Harris (2001, p. 38) describe the bimodal [Fe/H] distribution of the MW GCS. The latter fits a double Gaussian that peaks at [Fe/H] = -1.59 (metal-poor) and -0.51 (metal-rich) with dispersions of 0.34 and 0.23. T KMM mixture-modeling

Furthermore, We note that the scatter between different Auriga haloes is much smaller than the difference between the MW and M31 GCSs. We conclude that old star particles in the Auriga simulation suite as a whole cannot be consistent with both the Milky Way and the Andromeda globular cluster system.

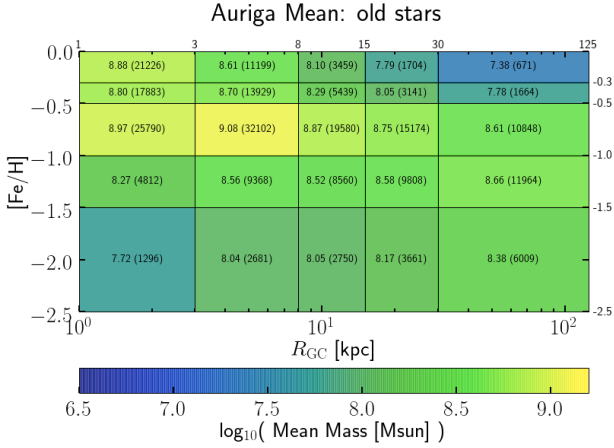We observe an increasing trend with increasing metallicity for

Figure 8. Mass-weighted [Fe/H]-R_{GC} distribution of all Auriga haloes (level 3, 4 and 5). Here we consider the old (> 10 Gyr) stars in all simulations and color-code the **mean value** (of 40 Auriga haloes)
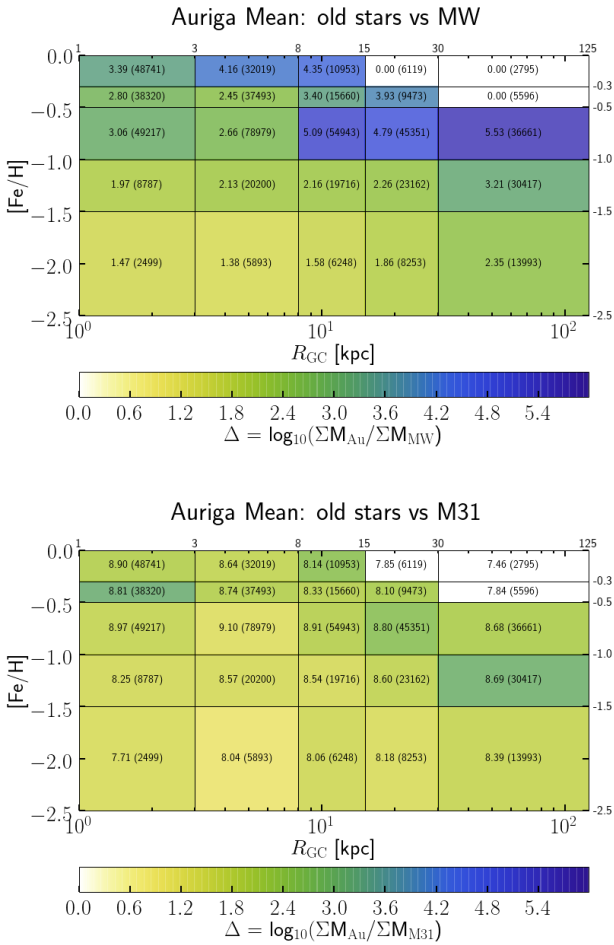

Figure 9. Caption

the Milky Way over the entire range of the data, while the M31 GCS shows this increase only in the range [Fe/H]>-0.5 (although not for the *old accreted* component.

Furthermore we test the null hypothesis that the metallicity distribution of the MW (M31) GCS and the *old*, *old insitu*, and *old accreted* star particles in the Auriga simulations are drawn from the same underlying distribution. We calculate the two-sample Kolmogorov-Smirnov test statistic for all thirty Auriga level 4 haloes and reject the null hypothesis for every halo, for every sub set of star particles at least at the 99.99% confidence level. In addition, the null hypothesis that the metallicity distributions of the MW and M31 GCS are drawn from the same distribution is rejected at the 99.99997% confidence level.

5.2 Radial distribution

> Harris: 'Somewhat arbitrarily, I will take the region $r_p > 3$ kpc (containing 75 clusters) as the fiducial Milky Way sample. If we were to view the Milky Way at the same inclination angle to the disk as we see M31, this cutoff in projected distance would correspond roughly to the inner distance limits in the M31 halo sample.'

5.3 Metallicity-radial space

See Figure 2 in Sec. 3.3.

> "The fraction of all star formation that occurs in bound stellar clusters (the cluster formation efficiency, hereafter CFE) follows by integration of these local clustering and survival properties over the full density spectrum of the ISM, and hence is set by galaxy-scale physics. We derive the CFE as a function of observable galaxy properties, and find that it increases with the gas surface density" (Kruijssen 2012)

5.4 Age cut

Although the age distribution of M31 Perhaps an age cut of 6 Gyr would would be more appropriate for M31, see Figure 1.

> Caldwell & Romanowsky (2016) writes: "there are two broad, well-established differences: (1) the M31 GC system is more populous than the MW system, by a factor of ~2-3, and (2) it does not exhibit the same obvious bimodality in metallicity (Barmby et al. 2000; Galleti et al. 2009; Caldwell et al. 2011; Cezario et al. 2013). Both of these aspects may be reflections of dramatic differences discovered in these galaxies stellar halos, where the M31 halo appears much more metal-enriched, with massive substructures suggesting a more active satellite accretion history (e.g. McConnachie et al. 2009)"

5.5 From star particles to globular clusters

Star particles are not globular clusters. Many stars do form in clusters, but not all clusters end up gravitationally bound. Star particles in the Auriga simulations represent single-age stellar populations that have formed at the same location within the galaxy. Therefore one could assume a model for the star cluster formation efficiency Γ, which could be used to 'convert' star particles to bound star clusters e.g. Kruijssen (2012). This model relies on the local birth properties of the star particles. However, in our analysis we can retrieve the

properties of the star particle in the first snapshot it was recorded, but not the gas properties at times of birth. Therefore we are unable to model the formation of star clusters in more detail.

Furthermore, we compare star particles to present-day globular clusters, thereby ignoring the effects of (dynamical) disruption of globular clusters over nearly a Hubble time. As shown by Pfeffer et al. (2018), a detailed model of the tidal history of star clusters requires a temporal resolution of order mega year. For the Auriga level 4 simulations we have 128 snapshots for the age of the Universe, thus, a far too coarse temporal resolution for meaningful calculations.

Therefore we investigate the over-production of simulated mass in the metallicity and radial bins and use the term 'efficiency' to refer to the combined product of bound cluster formation and globular cluster disruption. In Figure **??** we show the efficiencies that we find when we compare the simulations to the globular cluster systems of the Milky Way as well as that of Andromeda (M31).

6   SUMMARY AND CONCLUSIONS

REFERENCES

Ashman K. M., Zepf S. E., 1998, Globular Cluster Systems
Barmby P., Huchra J. P., Brodie J. P., Forbes D. A., Schroder L. L., Grillmair C. J., 2000, AJ, 119, 727
Brodie J. P., Strader J., 2006, ARA&A, 44, 193
Caldwell N., Romanowsky A. J., 2016, ApJ, 824, 42
Caldwell N., Schiavon R., Morrison H., Rose J. A., Harding P., 2011, AJ, 141, 61
Cezario E., Coelho P. R. T., Alves-Brito A., Forbes D. A., Brodie J. P., 2013, A&A, 549, A60
De Angeli F., Piotto G., Cassisi S., Busso G., Recio-Blanco A., Salaris M., Aparicio A., Rosenberg A., 2005, AJ, 130, 116
Faucher-Giguère C.-A., Lidz A., Zaldarriaga M., Hernquist L., 2009, ApJ, 703, 1416
Galleti S., Federici L., Bellazzini M., Fusi Pecci F., Macrina S., 2004, A&A, 416, 917
Galleti S., Bellazzini M., Buzzoni A., Federici L., Fusi Pecci F., 2009, A&A, 508, 1285
Grand R. J. J., et al., 2017, MNRAS, 467, 179
Harris W. E., 1996, AJ, 112, 1487
Harris W. E., 2001, Globular Cluster Systems. Springer Berlin Heidelberg, p. 223–408, doi:10.1007/3-540-31634-5_2, https://doi.org/10.1007/3-540-31634-5_2
Helmi A., 2008, A&ARv, 15, 145
Huxor A. P., et al., 2014, MNRAS, 442, 2165
Kruijssen J. M. D., 2012, MNRAS, 426, 3008
Mackey A. D., et al., 2019, MNRAS, 484, 1756
Marinacci F., Pakmor R., Springel V., 2014, MNRAS, 437, 1750
McConnachie A. W., et al., 2009, Nature, 461, 66
McLaughlin D. E., van der Marel R. P., 2005, ApJS, 161, 304
Pakmor R., Springel V., 2013, MNRAS, 432, 176
Pakmor R., Marinacci F., Springel V., 2014, ApJ, 783, L20
Pakmor R., Springel V., Bauer A., Mocz P., Munoz D. J., Ohlmann S. T., Schaal K., Zhu C., 2016, MNRAS, 455, 1134
Renaud F., Agertz O., Gieles M., 2017, MNRAS, 465, 3622
Ryu J., Lee M. G., 2018, ApJ, 863, L38
Springel V., 2010, MNRAS, 401, 791
Springel V., Hernquist L., 2003, MNRAS, 339, 289
Springel V., Di Matteo T., Hernquist L., 2005, MNRAS, 361, 776
VandenBerg D. A., Brogaard K., Leaman R., Casagrande L., 2013, ApJ, 775, 134
Veljanoski J., et al., 2014, MNRAS, 442, 2929
Vogelsberger M., Genel S., Sijacki D., Torrey P., Springel V., Hernquist L., 2013, MNRAS, 436, 3031
Wang S., Ma J., Liu J., 2019, arXiv e-prints
Zinn R., 1985, ApJ, 293, 424

APPENDIX A: SCATTER BETWEEN INDIVIDUAL AURIGA HALOES, AND NUMERICAL CONVERGENCE

We check whether the properties of the Auriga globular cluster candidates are well converged between the three different resolution levels used for the Auriga simulations. Here we consider all three Auriga haloes for which simulation runs were performed at all three resolution levels: Au6, Au16, and Au24. Here we can investigate differences between individual haloes.

Figure A1 shows the mass-weighted metallicity distribution, Figure A2 shows the mass-weighted radial distribution, and Figure **??**

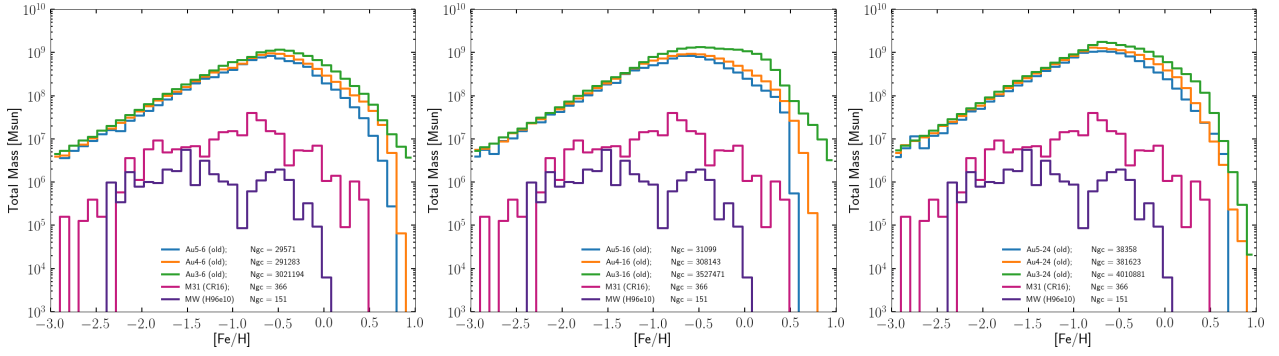This paper has been typeset from a TEX/LATEX file prepared by the author.

Figure A1. Same as Figure 5, but here the colours indicate resolution level: L3 green, L4 orange, and L5 blue. *Left:* Auriga halo 6. *Mid:* Auriga halo 16. *Right:* Auriga halo 24. For all three haloes we find marginal increases in the mass normalization with increasing resolution level.
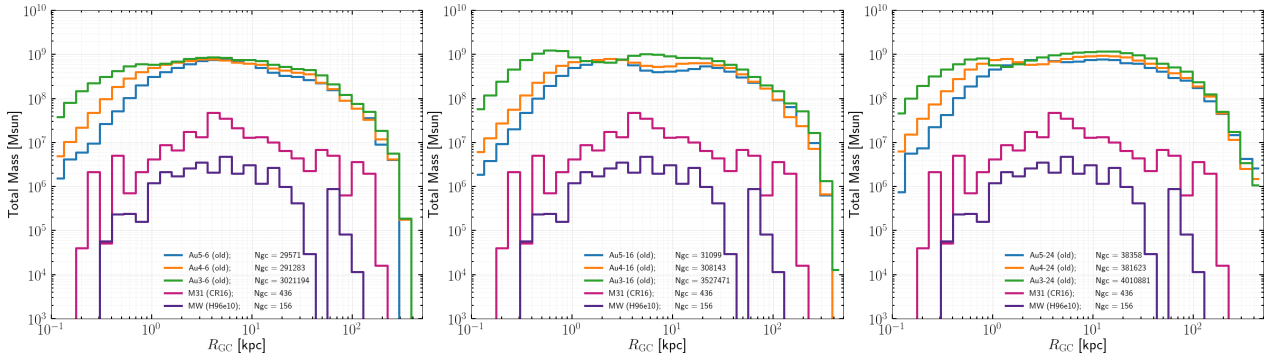

Figure A2. Same as Figure 7, but here the colours indicate resolution level: L3 green, L4 orange, and L5 blue. *Left:* Auriga halo 6. *Mid:* Auriga halo 16. *Right:* Auriga halo 24. For all three haloes we find marginal increases in the mass normalization with increasing resolution level.